Studying the topological organization of the cerebral blood flow fluctuations in resting state

Lester Melie-García [a,*], Gretel Sanabria-Diaz [b], Carlos Sánchez-Catasús [c]

[a] Neuroinformatics Department, Cuban Neuroscience Center, Cuba
[b] Clinical Neuroimaging Department, Cuban Neuroscience Center, Cuba
[c] Center for Neurological Restoration, Cuba

ARTICLE INFO

ABSTRACT

In this paper the cerebral blood flow (CBF) in resting state obtained from SPECT imaging is employed as a hemodynamics descriptor to study the concurrent changes between brain structures and to build binarized connectivity graphs. The statistical similarity in CBF between pairs of regions was measured by computing the Pearson correlation coefficient across 31 normal subjects. We demonstrated the CBF connectivity matrices follow 'small-world' attributes similar to previous studies using different modalities of neuroimaging data (MRI, fMRI, EEG, MEG). The highest concurrent fluctuations in CBF were detected between homologous cortical regions (homologous callosal connections). It was found that the existence of structural core regions or hubs positioned on a high proportion of shortest paths within the CBF network. These were anatomically distributed in frontal, limbic, occipital and parietal regions that suggest its important role in functional integration. Our findings point to a new possibility of using CBF variable to investigate the brain networks based on graph theory in normal and pathological states. Likewise, it opens a window to future studies to link covariation between morphometric descriptors, axonal connectivity and CBF processes with a potential diagnosis applications.

© 2012 Elsevier Inc. All rights reserved.

Introduction

The highly interconnected networks in the brain are capable of generating and integrating information from multiple sources in real time (Bassett and Bullmore, 2006). The characterization of the global architecture of these cerebral networks is crucial to understand how functional brain states emerge from the underlying structural substrate, and how the system maximizes the complexity of its function minimizing the costs (Sporns and Kotter, 2004).

Recent studies based on graph theory have found that the brain networks (at different spatial scales) follow the principle of the small-world topology associated with high global and local efficiencies of parallel information processing, sparse connectivity between nodes, and low wiring cost (Bassett and Bullmore, 2006). Several physiological and anatomical variables acquired through diverse Neuroimaging techniques have been successfully used in this purpose that conditional to its natures they extract different features of the brain networks. For instance, functional networks have been characterized by regional blood oxygenation levels (BOLD: blood oxygen level dependent) based on fMRI measurements (Achard et al., 2006; Bassettt et al., 2006; Wang et al., 2009), whereas electrical/magnetic signals recorded in sensors over/near the scalp through EEG/MEG techniques provide the information to study the coordinated electrical activity at the sources and sensors spaces (Micheloyannis et al., 2006; Stam, 2004; Stam et al., 2007). On the other hand, the Diffusion Weighted imaging (DWI) measuring indirectly the water diffusion in brain tissues, has been combined with fiber tracing methodologies to reconstruct anatomical (axonal connections) networks (Gong et al., 2009; Hagmann et al., 2007; Iturria-Medina et al., 2008). In addition, brain morphological networks are characterized using information of the synchronized co-variation patterns in morphometric variables like cortical thickness, surface area and volume (Bassett et al., 2008; He et al., 2007a; Sanabria-Diaz et al., 2010) obtained from high resolution anatomical MRI.

It is important to point out that these physiological variables (mentioned above) capture distinct properties of the interaction or different aspects of the same interaction (mechanical, anatomical, chemical, etc.) among cerebral regions revealing specific features of the brain networks architecture. In addition, its capabilities to differentiate normal from aberrant behaviors of human cerebral networks have been evidenced (Bassett et al., 2008; He et al., 2008, 2009a, 2009b; Iturria-Medina et al., 2011b).

The cerebral blood flow (CBF) is a different physiological variable used to study specific cerebral circuits principally the resting state networks (RSN). CBF has been imaged by Single-Photon Emission Computed Tomography (SPECT) and Positron Emission Tomography

(PET) both of which requires radioactive agents, as well as by the Arterial spin labeling (ASL) MRI technique (Detre et al., 1992).

The first network-based study resting on CBF was developed by Friston et al. (1993) using PET imaging. In this paper the distributed brain systems associated with performance of a verbal fluency task were identified through recursive Principal Component Analysis (rPCA) methodology. rPCA method groups brain regions into a few latent components. In particular, the brain regions within each component are believed to have strong connectivity, while the connectivity between components is weak.

The ASL technique has been utilized to measure dynamic, spontaneous CBF changes in resting state (Biswal et al., 1997; Chuang et al., 2008; De Luca et al., 2006; Wu et al., 2009). The pioneer study developed by Biswal et al. (1997) demonstrated that the spontaneous low frequency (<0.1 Hz) flow weighted fluctuations are highly synchronized within the motor cortex. The RSNs were studied by De Luca et al. (2006), where at least 5 distinct resting state network patterns were reproducible across different subjects. These RSNs appear to reflect 'default' interactions related to functional networks recruited by specific types of cognitive processes. More recently Chuang et al. (2008) developed a methodology to reduce BOLD contamination in the CBF measurements to find connectivity within the sensorimotor network. Additionally, Zou et al. 2009 showed the static and dynamic characteristics of the CBF in resting state have high correlation (functional connectivity) between components in the default mode networks (posterior cingulate cortex, thalamus, insula/superior temporal gyrus and medial prefrontal cortex) (Zou et al., 2009). On the other hand, Viviani et al. (2011) found a correspondence between BOLD and CBF connectivity maps (by Pearson correlation as an association measure) in a large sample of subjects ($N = 265$) using a set of seed structures like the intraparietal sulcus, middle temporal region and the posterior cingulated/precuneus. Surprisingly, we found only one work using CBF measurements obtained by SPECT imaging to characterize the functional connectivity (Okabe et al., 2003). Okabe et al. (2003) studied the motor cortex to other brain regions during repetitive transcranial magnetic stimulation (rTMS).

However, despite all studies developed to date one aspect is lacking in the literature so far: the study of the topological organization of the cerebral blood flow fluctuations in resting state. In other words, the topological features of the cerebral networks based on fluctuations of CBF hemodynamic variable have not been characterized yet in terms of the graph theory.

Additionally, SPECT imaging has never been used to characterize global brain networks while this technique provides valuable information to describe hemodynamic processes interactions between near and anatomically distant brain structures. In particular SPECT has been recognized as a reliable technique to measuring brain blood flow-based hemodynamics with a large number of applications at lower cost than PET (DeKosky and Scheff, 1990; Holman and Tumeh, 1990; Wintermark et al., 2005).

In the present study, we proposed to characterize CBF concurrent changes between pairs of brain regions as a new approach to study the brain networks. The statistical similarity between two regions was measured by computing the Pearson correlation coefficient. We explore for the first time the topological properties (global and local) of the CBF networks in resting state in a normal cohort of subjects. Our study could be another step to understand the organization of the human brain networks using a physiological variable barely explored. Next sections provide details about our study and its novelty.

Materials and methods

Subjects

A number of 31 right-handed healthy subjects (M) (mean age 60.32; range 50–77 years; standard deviation 6.6, 14 males and 17 females, mean instructions years 13.77).

MRI acquisition: high resolution anatomical imaging

For all subjects, a 3D high resolution T1-weighted anatomical image was acquired using a MRI scanner Siemens Symphony 1.5 T (Erlangen, Germany). A MPRAGE pulse sequence covering the whole brain was used with the following parameters: 160 contiguous slices of 1 mm thickness in sagittal orientation; in plane FOV $= 256 \times 256$ mm^2, and matrix size 256×256 yielding an in plane spatial resolution of 1×1 mm^2 and voxel size of $1 \times 1 \times 1$ mm^3. The echo time, repetition time and inversion time were set to TE/TR/TI $= 3.93$ ms/3000 ms/1100 ms with a flip angle FA $= 15°$.

SPECT acquisition

SPECT imaging was performed with a double-head system (DST Xli, Sopha Medical Vision, France) equipped with ultra-high-resolution fan-beam collimators. The measured tomographic resolution for ^{99m}Tc was 8.5 mm in the center of the image at the fixed radius of rotation of 150 mm. The imaging was started 10 min after injection of 555 MBq of ^{99m}Tc-ethyl cysteinate dimer into the antecubital vein of the right arm under resting condition (supine, eyes open, dimly lit quiet room). Projection data were obtained for each camera in a 128×128 format for 64 angles at 26 s per angle. Total counts were equal or greater than 5×10^6. A Butterworth filter was used for image back-projection reconstruction of SPECT images (cutoff frequency $= 0.026$ cycle/cm and order $= 7$). Attenuation correction was performed using Chang's method (Chang, 1978) with attenuation coefficient $\mu = 0.085$ cm. The reconstructed images have in-plane spatial resolution of 128×128 pixels, yielding a voxel size of 3.5 mm $\times$ 3.5 mm $\times$ 3.5 mm. SPECT and MRI were carried out with a maximum interval of one week.

Data preprocessing: CBF matrix computation

SPECT images were corrected for partial volume effect (PVE) using the modified Müller–Gartner voxel-based method (Quarantelli et al., 2004). All preprocessing steps for PVE correction were carried out by the 2010-version of the 'PVE-lab' software (http://pveout.area.na.cnr.it). Each PVE-corrected SPECT image was coregistered onto its respective native GM segment using the normalized mutual information procedure with trilinear interpolation by SPM8 (http://www.fil.ion.ucl.ac.uk/spm). Coregistered SPECT images were normalized to MNI space including the 12 mm smoothing kernel. The resulting SPECT images were then scaled by the mean gray matter activity from vermis (cerebellum), which were automatically extracted using the IBASPM toolbox (Individual Brain Atlases using the Statistical Parametric Mapping (SPM) available at http://www.fil.ion.ucl.ac.uk/spm/ext/#IBASPM) (Alemán-Gómez et al., 2006) and the anatomical labeling template (Tzourio-Mazoyer et al., 2002). At last step, Lassen correction (back diffusion model for linearization) was applied to eliminate the underestimation of regional CBF due to the limited first-pass extraction of the tracer or back diffusion of the tracer from the brain (Lassen et al., 1988). These corrected SPECT images were used to study CBF networks.

Using IBASPM toolbox the GM tissue of the T1-weighted images were automatically segmented into a parcellation with $N = 90$ anatomical structures using the AAL atlas (Tzourio-Mazoyer et al., 2002). More details about the atlas structure names can be found in Supplementary Material A. The parcellation process was conducted to the SPECT native space, where the mean CBF in all anatomical structures were calculated. This process was performed for all subjects yielding a matrix with 'M' rows (number of subjects) by 'N' columns (number of structures) of CBF values for the AAL parcellation (Fig. 1 represents schematically the CBF data matrix construction).

Connectivity matrix construction for CBF

We defined a connection as statistical associations in CBF between brain regions for a particular parcellation (see Fig. 2). The statistical

similarity between two regions was measured by computing the Pearson correlation coefficient, across subjects. Hence, the interregional correlation matrix ($N \times N$, where N is the number of brain regions, here $N = 90$) of such connections was obtained for all pairs of anatomical structures. The element c_{ij} is the value of the Pearson correlation between regions i and j (see Fig. 2). Self-connections were excluded, implying a diagonal black line in the symmetric matrix. Only those correlation coefficients statistically significant (p value<0.05) were taken into account for studying the CBF network. Prior to the correlation analysis, a linear regression was performed at every region to remove the effects of age, gender, age–gender interaction, and overall CBF (sum of the all structure's CBF). For the CBF matrix, the residuals of this regression was then substituted for the raw values respectively (see Fig. 2, step 2).

Similar to our previous paper based on morphological connectivity (Sanabria-Diaz et al., 2010) we obtained bootstrapping samples of the connectivity matrix selecting a random subset of the total number of subjects to compute the Pearson correlation coefficient. Through this procedure, it was possible to study the changes of network properties taking into account the variability of having different combinations of subjects in the sample. In particular we acquired 300 bootstrap samples using a subset that contains 80% of the total number of subjects (24 subjects).

The connectivity matrices were thresholded to create sparse graphs (Fig. 2, step 5). Rather than restricting our analysis to a binarized

graph obtained by applying a single threshold value, we explored the properties of the graphs over a range of thresholds to explore metrics with different sparseness. The threshold values R_k were calculated to obtain different matrix sparseness that we denote as 'sparsity degree'. A sparsity degree of 0.9 means that 90% of the connectivity matrix is off, and only the highest 10% of the connectivity values were taking into account. The R_k were computed for sparsity degrees ranging from 0.5 to 0.9, in step of 0.02, yielding a set of 21 threshold values. This procedure normalizes the networks to have the same number of nodes and edges, allowing the examination of the relative network properties obtained. In these matrices (see Fig. 2, steps 5 and 6), an element was set to 1 if, the absolute value of the CBF correlation between two regions i and j denoted by c_{ij} was higher than R_k; $|c_{ij}| > R_k$ and 0 otherwise. This binarized connectivity matrix captures the underlying connection patterns of the human brain common to the population sample under study.

Graph analysis to characterize brain CBF connections

A great number of natural systems can be represented by complex networks. Graph Theory is usually considered an attractive model for the mathematical treatment of brain network connectivity. In general, a complex network can be represented as a graph $G = [N, K]$, the components of this system are called nodes (N) and the relations or connections between them are called edges (K) (Boccaletti et al., 2006). In our
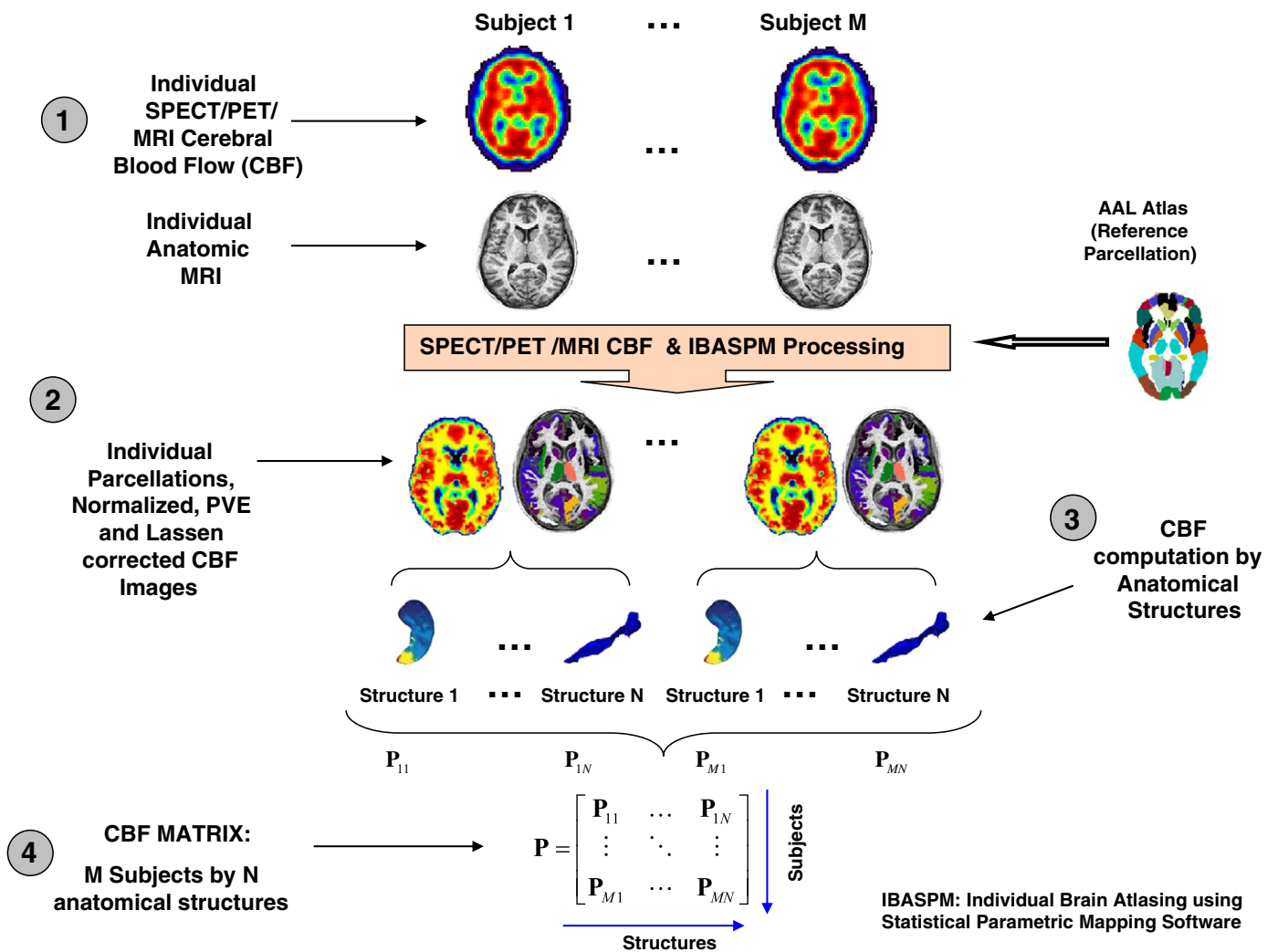

Fig. 1. Flowchart of the CBF matrix construction. 1) Representation of the individual CBF/Anatomic brains for all subjects. 2) After IBASPM processing, using AAL atlas the individual parcellations for the M subjects are obtained. 3) The mean CBF was computed for the 'N' anatomical structures. 4) The CBF values for each anatomical structure were organized in an array, given the final CBF matrix denoted by 'P' with 'M' rows by 'N' columns.
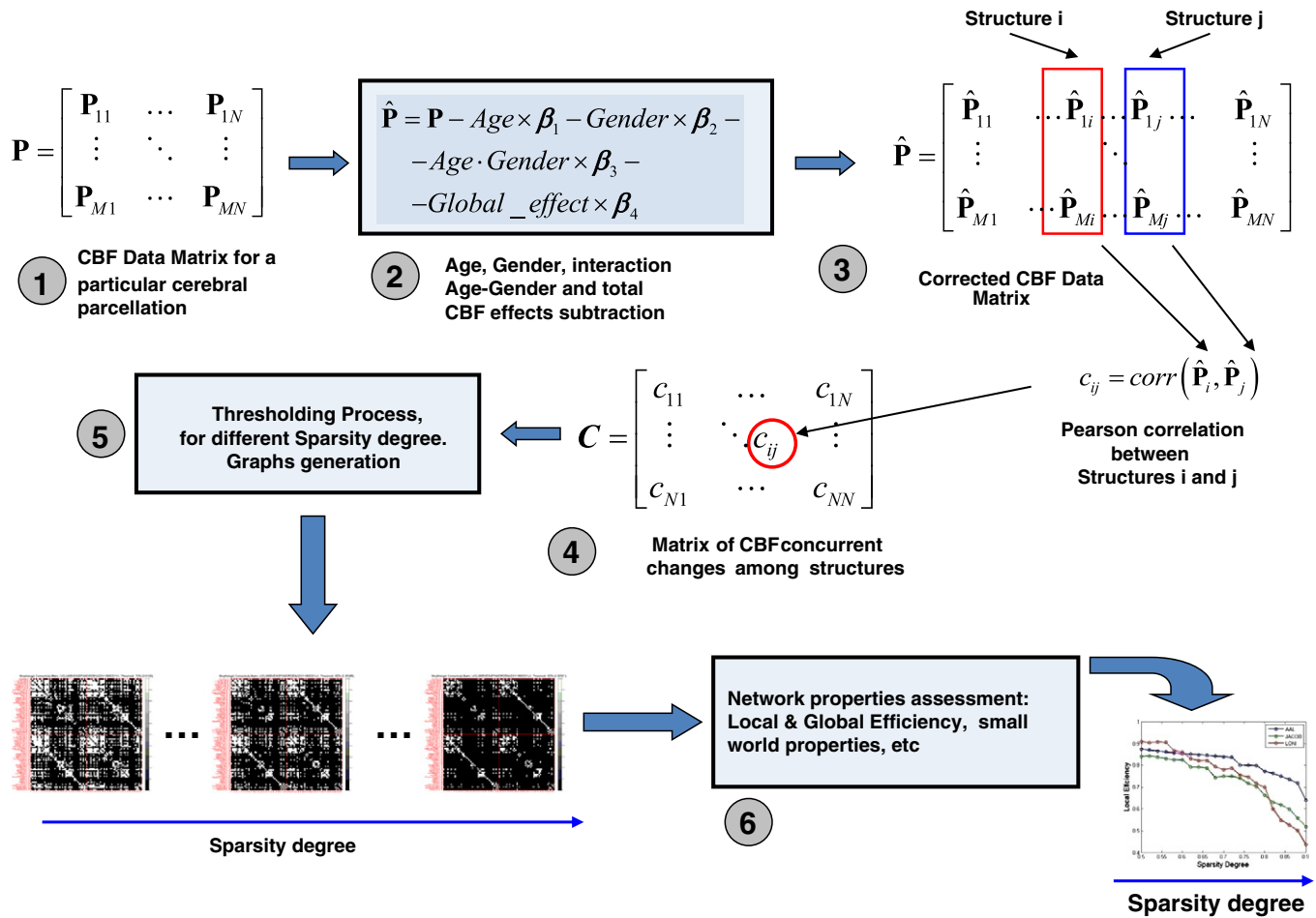
Fig. 2. Steps for computing CBF connectivity matrices. 1) CBF Data matrix. 2) The data matrix was substituted by residuals of the linear regression subtracting effects of age, gender, interaction age-gender and the global effect (total CBF) represented in 3). 4) Correlation matrix representing the concurrent changes among all pairs of anatomical structures. 5) Thresholding process for different sparsity levels to generate binary graphs. 6) Assessment of the network properties for all binary graphs obtained in 5).

specific case, the brain network is considered unweighted because all edges are assumed to indicate relations of equivalent strength between nodes, and undirected, since it summarizes symmetric relations (such as correlations) between nodes.

We estimated the most important local and global metrics of the graph G. The computed global network properties were: small-world attribute (sigma), cluster index, local and global efficiencies and characteristic path length. On the other hand to describe local properties the betweenness centrality measure was used. The description of these graph attributes can be found elsewhere (Rubinov and Sporns, 2010).

Results

Connections between interhemispheric homotopic cerebral regions

Using the methodology described above, the matrix of CBF concurrent changes between brain anatomical structures was estimated. The existence of connections between homotopic interhemispheric cerebral regions which is in accordance with the existing anatomical knowledge (see Fig. 3) (Gómez-Padrón et al., 1985; Standring, 2004; Witelson, 1989) and previous anatomical, functional and morphological connectivity studies using graph theory (He et al., 2007a, 2008; Mechelli et al., 2005; Salvador et al., 2005; Stark et al., 2008; Yao et al., 2010) should be noted. It is important to point out that these connections, in special between homologous regions, presented the highest correlation values (see Fig. 4).

CBF synchronized co-variations among brain anatomical structures

Table 1 shows the 15 strongest CBF co-variations among anatomical regions defined in the AAL atlas. Most of them were between pairs of homotopic regions mainly associated with several parts of corpus callosum. In addition, we found these connections were more numerous than those between non-homotopic regions. This result is consistent with previous resting-state network studies (Salvador et al., 2005; Stark et al., 2008) showing a robust correlated spontaneous activity between homotopic regions. The strongest intrahemispheric CBF co-variations are related with several major white matter tracts (e.g., superior longitudinal fasciculus). These long-range connections might play roles as shortcuts to ensure short mean path lengths in the small-world networks (Hilgetag and Kaiser, 2004). Also we found pairs of regions with high CBF co-variations that are connected via short-range white matter fiber bundles like the arcuate fasciculus.

Global properties of the CBF network

Recently, several papers studying brain networks features based on different neuroimaging modalities (MRI (sMRI), fMRI, EEG, MEG) and graph theory have demonstrated the cerebral functions emerges from the topology of the network as a whole. In special, a 'small-world' topology is observed in the human brain networks exhibiting (high clustering and short path lengths) a set of hub regions predominantly located in heteromodal association cortical areas (Achard and Bullmore, 2007;
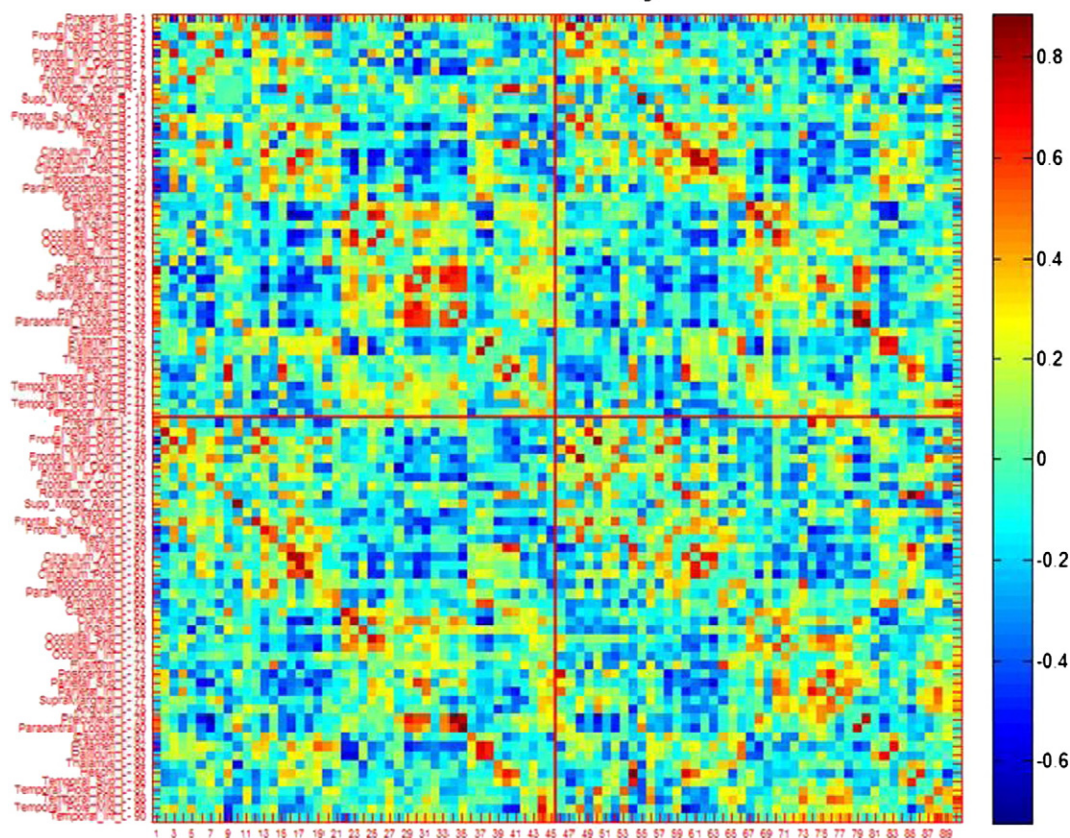
CBF Connectivity Matrix

Fig. 3. The CBF connectivity matrix obtained by calculating Pearson's correlation between regional CBF across subjects. The color bar indicates the correlation coefficient value. (For interpretation of the references to color in this figure legend, the reader is referred to the web version of this article.)

Achard et al., 2006; Bassett et al., 2008; Bassettt et al., 2006; Deuker et al., 2009; Eguiluz et al., 2005; Gong et al., 2009; Hagmann et al., 2008; He et al., 2007a, 2007b; Liu et al., 2008; Micheloyannis et al., 2006; Salvador et al., 2005; Stam, 2004; Stam and Reijneveld, 2007; Stam et al., 2007; van den Heuvel et al., 2008).

In present study, the CBF network properties (clustering index, characteristics path length, local efficiency, global efficiency and sigma) were calculated over a range of sparsity values (from 0.4 to 1.0) (see Materials and Methods section for details) as is illustrated in Fig. 5. As expected, the CBF network exhibited small-world attributes overall range of sparsity degree values (Fig. 5, panel D).

Nodal properties of the CBF network

In order to study the nodal properties (betweenness centrality) the CBF network, was constructed at a sparsity degree of 89%. This selection has been used by previous papers and ensures that all regions have at least one connection, minimizing the number of false-positive paths and optimizing interregional correlation strengths (see Fig. 6 and Supplementary Material C) (Bassettt et al., 2006; He et al., 2008; Yao et al., 2010). Next sections show the principal findings in this nodal attributes study.

Nodal betweenness centrality

We calculated the normalized betweenness centrality (NBC) of each region in the CBF network shown in Fig. 6. Cortical regions with high NBC are important in managing the flow of information across the network due to they are more likely to reside on the shortest paths

between other regions. We found 20 structures with NBC values higher than 1.51 (22% of cerebral regions) with a maximum of 3.84 in the frontal middle orbital of the right hemisphere (see Supplementary Material C for full regions list and its respective normalized betweenness centrality values). These regions involve the cingulate cortex, as well as portions of frontal, inferior and superior parietal cortices, and middle and superior occipital cortices (Fig. 6). It was observed that these brain structures were equally distributed in both cerebral hemispheres. Finally, we also found, as expected, an increment of the mean betweeness centrality of the CBF network with the sparsity degree.

Hub regions

In general, hubs in a particular network are identified as those with a betweenness centrality (BC) values at least 1.5 times greater than the average BC ($<BC>$) of the network (i.e., $BC > 1.5^* <BC>$). In our case, the CBF network presents twenty hub regions (for details, see Table 2). These included eight regions in the paralimbic cortex (cingulate gyrus, insula), six belonging to the heteromodal ones (precuneus, superior frontal gyrus), and four to the unimodal association cortex (superior occipital gyrus, cuneus). The other two hub regions were localized in the primary cortex (postcentral gyrus, calcarine fissure and surrounding cortex). Based on the subdivision of the cerebral cortex into five major functional subtype's areas, hubs in the CBF network showed an asymmetric pattern. Particularly, the heteromodal hubs prevailed in the left hemisphere contrary to the paralimbic and primary ones that were principally localized in the right hemisphere. On the other hand, hubs belonging to the unimodal cortex were equally distributed in both hemispheres.
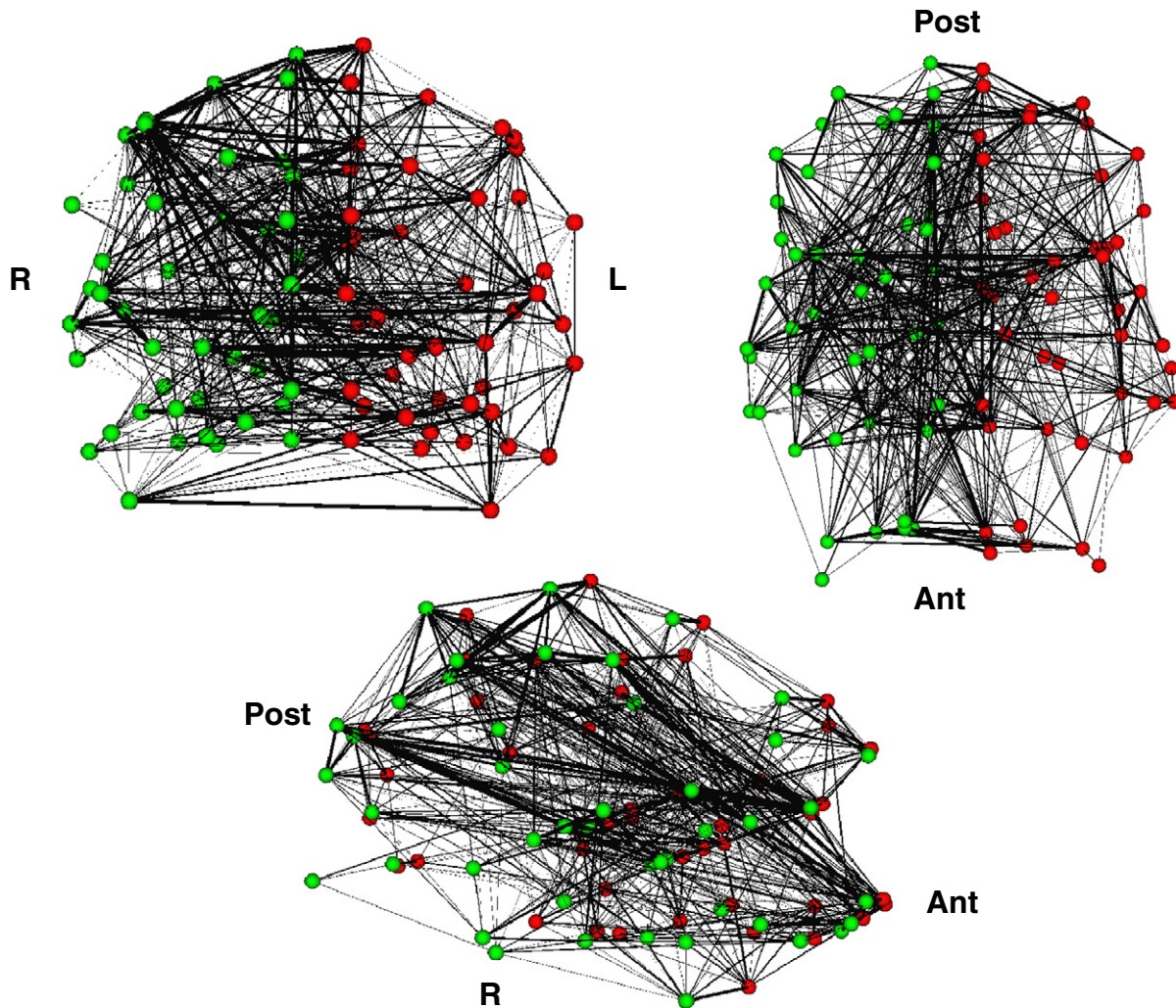
Fig. 4. The CBF networks (only the 700 strongest connections were represented). Line thickness indicates the strength of the connection. Red and green dots represent structures belonging to the right and left hemispheres respectively. Post: posterior, Ant: anterior, L: left, R: Right. (For interpretation of the references to color in this figure legend, the reader is referred to the web version of this article.)

This spatial distribution of hubs is in line with previous studies using other connectivity analysis (anatomical, functional and morphological) showing the existence of structural core regions positioned on a high proportion of shortest paths within the network (Achard et al., 2006; Bullmore and Sporns, 2009; Chen et al., 2008; Gong et al., 2009; Hagmann et al., 2008; He et al., 2007a, 2008, 2009b; Iturria-Medina et al., 2008; van den Heuvel and Sporns, 2011). Remarkably, these regions also agree with the ones obtained in previous vulnerability analysis (to identify hubs) like in Iturria-Medina et al. (2008). In contrast, the hubs with smallest NBC included regions of the paralimbic and unimodal cortices such as the olfactory, occipital inferior and orbitofrontal regions (for details, see Supplementary Material C). Similar to the result reported in the previous subsection with respect to the mean betweenness centrality, the number of hubs increases with the sparsity degree.

Discussion

In this work, the CBF synchronized co-variations among cerebral structures were used to study the human brain networks topology in resting state. As in previous papers (Bassett et al., 2008; He et al., 2008, 2009b) the behavior of the network properties (clustering index, characteristic path length, small-world attributes (sigma) and local and global efficiency) were studied in a range of sparsity values.

The principal contributions of this paper can be summarized as follows:

1. The CBF is a physiological variable that provides valuable information to study the topological organization of human brain functional networks in resting state.
2. The pattern of the concurrent CBF fluctuations among cerebral regions shows a topology with 'small-world' attributes. This means that CBF network present an optimal balance between local specialization and global integration processes.
3. The principal CBF concurrent fluctuations are related to neuroanatomical pathways of the human brain (e.g. superior longitudinal fascicle (SLF) and corpus callosum (CC)).
4. The strongest synchronized fluctuations in CBF were found between homologous cortical regions (connected through CC).
5. The existence of a functional core (hubs) positioned on the high proportion of shortest paths within the CBF network. These were anatomically distributed in frontal, limbic, occipital and parietal regions suggesting its important role in functional integration. This fact has been previously reported studying anatomical (structural core) and functional networks based on DWI and fMRI neuroimaging techniques.

Some of these findings deserve more attention and will be discussed in the following subsections.

Table 1
The 15 strongest interregional blood flow correlation values (connections) and their approximate associated fiber tracts.

No	Region A	Region B	Class	R	Approximate associated fiber tracts
1	Paracentral Lobule L	Paracentral Lobule R	SIH	0.89	Genu and anterior part of the body of CC[2]
2	Heschl gyrus L	Rolandic operculum L	IH	0.88	Superior longitudinal fasciculus (arcuate fascicle) [5]
3	Precuneus L	Precuneus R	SIH	0.84	Part of the body and the splenium of CC[1,2]
4	Supplementary motor area L	Supplementary motor area R	SIH	0.83	Anterior midbody (anterior half) of the CC[1,3]
5	Middle frontal gyrus, (orbital part) L	Middle frontal gyrus, (orbital part) L	IH	0.81	Superior longitudinal fasciculus (U fibers)[4]
6	Anterior cingulate and paracingulate gyri L	Anterior cingulate and paracingulate gyri R	SIH	0.81	CC[7]
7	Postcentral gyrus R	Precentral gyrus R	IH	0.80	Arcuate fibers[7]
8	Pallidum R	Putamen R	IH	0.78	Striatopallidal fibers[6]
9	Median cingulate and paracingulate gyri L	Median cingulate and paracingulate gyri R	SIH	0.77	CC[4, 7]
10	Precuneus L	Paracentral Lobule R	NIH	0.77	N/A
11	Anterior cingulate and paracingulate gyri L	Median cingulate and paracingulate gyri R	NIH	0.76	CC[4]
12	Superior frontal gyrus, (dorsolateral) L	Superior frontal gyrus, (dorsolateral) R	SIH	0.76	Genu and anterior part of the body of CC[1,2]
13	Paracentral Lobule L	Precuneus L	IH	0.75	Superior longitudinal fasciculus (SLFI)[5]
14	Cuneus L	Cuneus R	SIH	0.75	Inferior part of the splenium of CC[1,2,3]
15	Superior occipital gyrus L	Superior occipital gyrus R	SIH	0.74	Posterior part of the splenium of CC[1,2,3]

L.: Left R.: Right CC: corpus callosum N/A: unclear or ambiguous WM tracts.
Note: List of the 15 strongest connections (descending order by correlation coefficient values). These connections were classified into intrahemispheric (IH), symmetrically interhemispheric (SIH) and asymmetrically interhemispheric (NIH). Column R denotes the correlation coefficients between regions. Approximate associated fiber tracts between each pair of regions observed in this study is listed in the right most column. (Full names of anatomical structures can be found in Supplementary Material A).
[1]Hofer and Frahm, 2006; [2]Huang et al., 2005; [3] Zarei et al. 2006; [4] Wakana et al. 2004; [5] Makris et al. 2005; [6] Mesulam, 2000; [7]Jellison et al. 2004.

The CBF can be used as a physiological variable to reveal the complex architecture of the human brain networks in resting state

Why could CBF be a suitable physiological descriptor to study properties of the cerebral networks in resting state? The answer to this question could be found by means of the well-known neurovascular coupling phenomenon.

It is known that local cerebral blood flow is regionally heterogeneous. The varied pattern of CBF is neither random nor related to the anatomic organization of the cerebral vasculature or to differences in the innervation patterns of the cerebral vessels. Neuronal activity is the principal energy-consuming process in the brain. Local cerebral blood flow adjusts to the level of energy generation; therefore, it is the activity in the neuronal circuits that is the major determinant of variations and regional patterns of cerebral blood flow. From the prospect of energy consumption, the human brain is a large energy consuming organ that represents about 2% of body weight, while accounting for 20% of the total body energy consumption. Furthermore, it is noteworthy that much of the brain's energy consumption is not attributed to external stimuli but to intrinsic or resting state activity (Raichle, 2006).

Therefore studying the synchronized CBF fluctuations between anatomical regions is able to have a functional connectivity measure among these brain sites in resting state.

On the other hand, since CBF is a single physiological parameter (vs. BOLD which is a composite of several parameters) and is probably more closely related to cerebral metabolism than BOLD, CBF data may be more physiologically relevant than those from BOLD (Zou et al., 2009). Functional connectivity studies using MRI have been almost exclusively performed by measuring the fluctuations in the BOLD weighted signal. BOLD signal fluctuations represent combined changes in blood oxygenation, cerebral blood volume, cerebral blood flow (CBF) and metabolic rate of oxygen (Buxton et al., 2004). Besides, the magnitude of BOLD fluctuation is also dependent on MRI specific parameters, such as magnetic field strength and echo time (TE). In contrast, functional connectivity mapping based on CBF provide a quantitative estimate of the fluctuations in terms of a single physiological parameter (Chuang et al., 2008).

Cerebral blood flow co-variations and its associated neuroanatomical pathways

In this study, it was found patterns of covariations in CBF between anatomical brain regions. One issue of interest is whether these set of

concurrent fluctuations are also related to known neuroanatomical pathways of the human brain. Findings in Varkuti et al. (2011) support this idea. The authors in this paper reported that anatomical connectivity and CBF are systematically linked throughout a number of brain regions. These results constitute a starting point for further research on the role of homology in the formation of functional connectivity networks and on how structure/function relationships can manifest in the form of such trait interdependency. Additionally, such coupling would constitute the manifestation of a supply-and-demand-principle — the metabolic demand being shaped by connectivity — in the formation of a structure/function relationship (Varkuti et al., 2011).

Here, we matched the 15 pairs of regions with the highest concurrent changes to the approximate associated anatomical connections obtained from previous human and animal diffusion imaging and tracing studies (see Table 1). We found an interesting set of regions with high covariations in CBF following the interhemispheric middle line of the brain. These anatomical regions are present from the occipital lobe (superior occipital gyrus), parietal (precuneus), supplementary motor area to frontal cortex (superior frontal gyrus). This pattern could be linked to the so-called rich-club phenomenon (van den Heuvel and Sporns, 2011) that assumes the existence of a number of highly connected and highly central hub regions that play a key role in global information integration between different parts of the network. Our hypothesis rest on that the maximal covariation in CBF across these particular set of inter-hemispheric homologous regions show indirectly their metabolic cost in order to support a global connectivity of the brain network as a kind of scaffolding. These ideas are in line with previous human brain functional studies that have demonstrated strong functional correlations between bilaterally homologous regions (Hampson et al., 2002; Lowe et al., 1998; Wang et al., 2006) and a similar symmetric clustering connectivity pattern (Salvador et al., 2005). The high covariations values (Pearson correlation coefficients) present between homologous regions can be explained by the associations of these regions through the corpus callosum (CC), a crucial white matter structure providing communications between both brain hemispheres. The anatomical localization across different lobes agrees with the transit of inter-hemispheric pathways connecting homologous brain areas (Hofer and Frahm, 2006; Huang et al., 2005; Zarei et al., 2006) and the in vivo parcellation of CC into several major subdivisions such as the genu, body and splenium.

We also observed a significant covariation in blood flow between intrahemispheric structures with different patterns for the left and
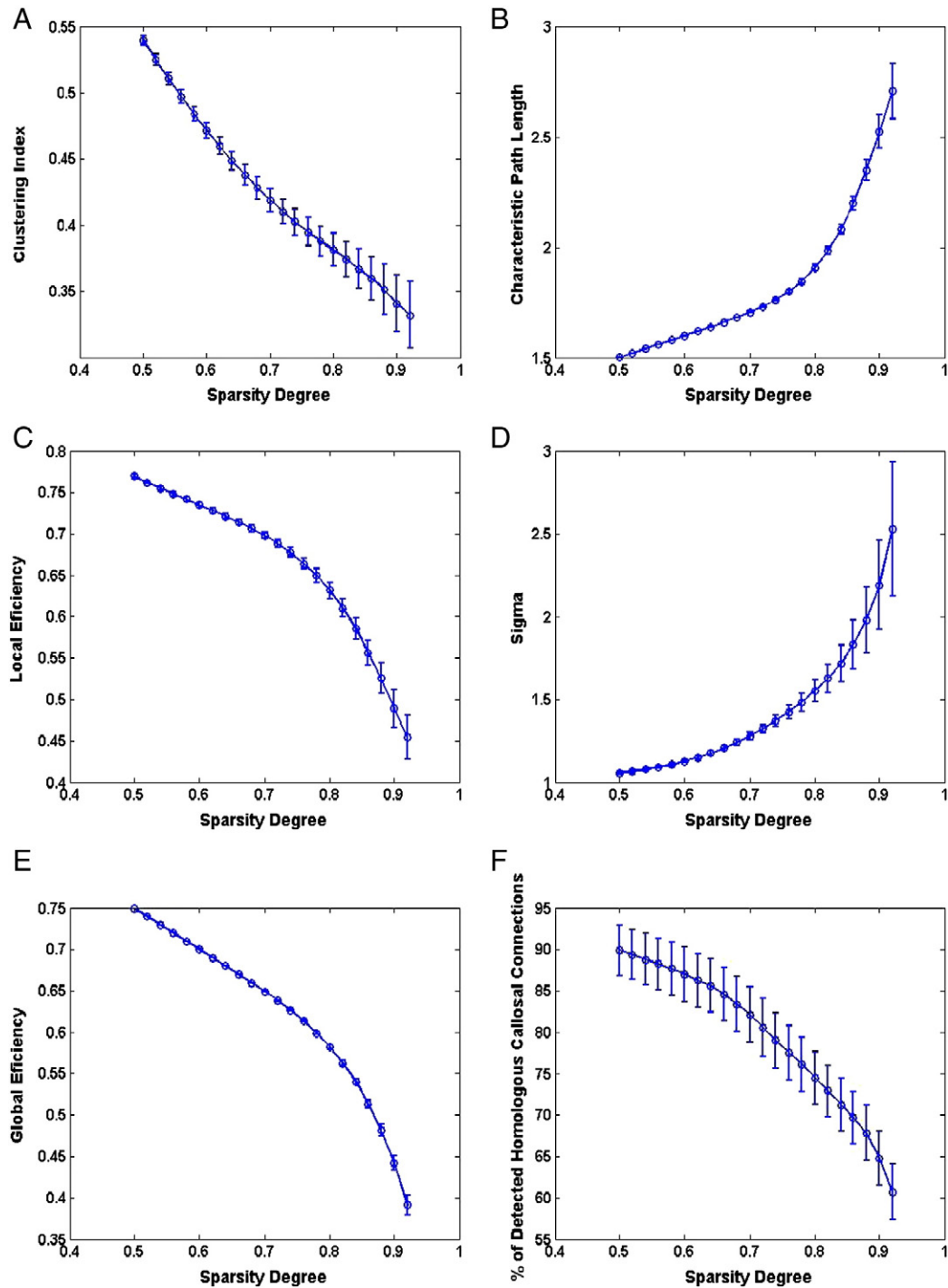
Fig. 5. Global network properties as function of sparsity degree. (A) The clustering index decreases as the sparsity degree increases (B). The characteristic path length increases as sparsity degree increases. (C) Local efficiency and global efficiency (E) decrease with sparsity degree. (D) Small-world attribute increases with sparsity degree. (F) Percent of detected homotopic callosal connections.

right hemispheres. Previous studies have reported structural and functional asymmetries in several regions of human cortex, including frontal, temporal, and occipital regions (for a review, see Toga and Thompson, 2003). Furthermore, Mechelli et al. (2005) have also demonstrated interregional asymmetric patterns of associations in gray matter concentration, providing further support to our finding of different connection patterns between both brain hemispheres. More recently, Iturria-Medina et al. (2011a) showed in both human and nonhuman primate brains, in terms of the graph theory, that the right hemisphere is significantly more efficient and interconnected than the left one, whereas the left hemisphere presents more central or indispensable

regions (hubs) for the whole-brain structural network than the right hemisphere.

In the present work, the anatomical connections between left hemisphere regions (e.g., heschl gyrus–rolandic operculum) are associated with the superior longitudinal fascicle (SLF) linking the caudodorsal prefrontal cortex with the premotor, supplementary motor, and superior parietal regions (Makris et al., 2005; Wakana et al., 2004). The CBF concurrent fluctuations between adjacent areas (e.g., middle frontal gyrus–superior frontal gyrus, orbital part) are examples of the presence of short association fibers (e.g., U-fibers) that provide the 'wiring' (anatomical substrate) which these areas could use to interact each other (Petrides,
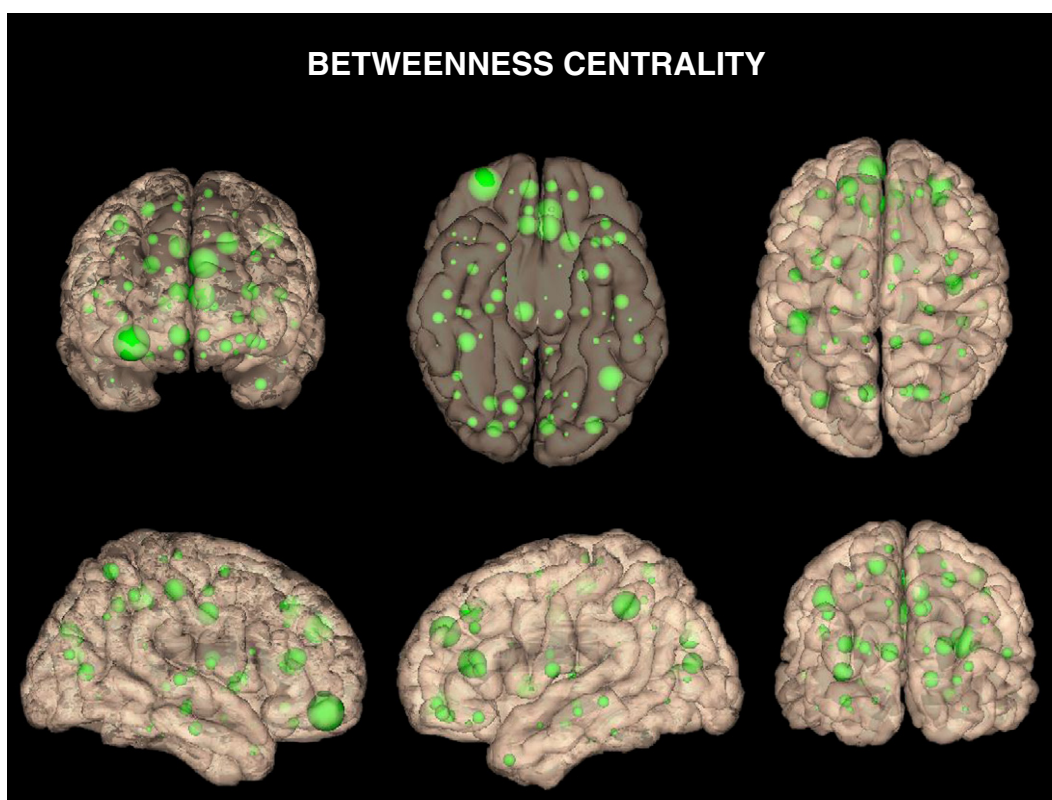
Fig. 6. Betweenness centrality values distribution in the cerebral cortex. This result was obtained for a sparsity degree of 89%. The spheres in green represent the cortical regions and its diameter the betweenness centrality value. The higher betweenness centrality index the larger the sphere's diameter. Full structure names and its respective normalized betweenness centrality values can be found in Supplementary Material C. (For interpretation of the references to color in this figure legend, the reader is referred to the web version of this article.)

2005; Wakana et al., 2004). Additionally, we also observed strong CBF synchronized fluctuations in the right hemisphere between subcortical nuclei (e.g., pallidum-putamen) connected via striato-pallidal fibers. For example, the lateral pallidum and the dorsal parts of the medial pallidum receive their striatal input predominantly from the caudate and putamen.

As noted above, we found CBF covariations between regions linked through short-range/local connections (associated through short fibers for instance arcuate or U-fibers, that constitute the local circuitry), long-range connections (related to commissural fibers: inter-hemispheric connections) and intra-hemispheric association fibers (e.g., SLF) (Wakana et al., 2004). Recent functional connectivity studies based on fMRI have demonstrated the presence of local and long-range connections in the human brain (Achard et al., 2006; Salvador et al., 2005) consistent with our results.

Summarizing, the CBF network analysis provides evidences on the true anatomical or functional connections among neural processing units and their activities.

Attributes of the cerebral blood flow network in resting state

This is the first study, to our knowledge, that demonstrates the presence of large-scale blood flow connectivity patterns in the human brain using SPECT imaging. Fig. 5 shows, as in previous studies (Bassett et al., 2008; He et al., 2008, 2009b), the dynamic of the network properties curves (clustering index, characteristic path length, small-world attributes (sigma), and local and global efficiency) in a range of sparsity degrees. We found that the human CBF network present 'small-world' attributes. This fact has been documented by the existing mammalian cortical networks derived from chemical tracing methods (Sporns and Zwi, 2004) and the recent human structural networks derived from diffusion MRI and MRI-based cortical thickness that have consistently

exhibited small-world attributes (Bassett et al., 2008; Gong et al., 2009; Hagmann et al., 2007; He et al., 2007a; Iturria-Medina et al., 2008; Sanabria-Diaz et al., 2010). Additionally, recent studies have demonstrated small-world properties in human brain functional networks using neurophysiological data, coming from fMRI (Achard et al., 2006; Eguiluz et al., 2005; Salvador et al., 2005), EEG (Micheloyannis et al., 2006; Stam et al., 2007), and MEG neuroimaging modalities (Stam, 2004).

In the present study, it was observed small-world properties were salient at medium-high sparsity degrees. Previous computational simulations have demonstrated that small-world topologies emerge when networks are evolved for high complexity (Sporns et al., 2000).

Summarizing, our results provide a comprehensive description of the network arisen from CBF concurrent fluctuations among brain regions. The small-worldness model showed by the CBF network indicates the high local interconnectivity or cliquishness and short mean distance between regions revealing a high efficiency in the communication between different parts in the network.

Hub regions and bridge connections in the CBF network

Based on normalized betweenness centrality measure, 20 hub regions were identified in the CBF network (see Table 2). We classified these regions in primary, unimodal, heteromodal, and paralimbic hubs. This result is compatible with previous reports studying brain functional, anatomical and morphological networks. It suggests that the spatial distribution of hubs is conserved and it is an invariant parameter of brain network organization at different scales and neuroimaging techniques (Achard et al., 2006; Bassett et al., 2008; Hagmann et al., 2008; He et al., 2007a; Iturria-Medina et al., 2008; van den Heuvel and Sporns, 2011).

Table 2
Principal hub regions classified as the primary, unimodal, heteromodal, paralimbic, limbic, or subcortical as described in Mesulam (2000).

Regions	NBC	Localization	Class
Middle frontal G (orbital part). R	3.84	Frontal lobe, orbital surface	Paralimbic
Superior frontal G (medial). L	3.23	Frontal lobe, medial surface	Heteromodal
Anterior cingulate G. L	2.99	Limbic lobe	Paralimbic
Inferior parietal. L	2.93	Parietal lobe	Heteromodal
Superior frontal G (dorsolateral). L	2.47	Frontal lobe	Heteromodal
Median cingulate G. R	2.34	Limbic lobe	Paralimbic
Postcentral G. R	2.31	Central region	Primary
Anterior cingulate G. R	2.29	Limbic lobe	Paralimbic
Superior frontal G (medial orbital). R	2.28	Frontal lobe, orbital surface	Paralimbic
Middle occipital G. L	2.13	Occipital lobe, lateral surface	Heteromodal
Superior occipital G. R	2.04	Occipital lobe, lateral surface	Unimodal
Cuneus. L	2.03	Occipital lobe, medial and inferior surfaces	Unimodal
Calcarine fissure. R	1.89	Occipital lobe, medial and inferior surfaces	Primary
Insula. L	1.87	Insula	Paralimbic
Superior parietal G. R	1.79	Parietal lobe, lateral surface	Unimodal
Rolandic operculum. L	1.71	Central region	Unimodal
Precuneus. R	1.62	Parietal lobe, medial surface	Heteromodal
Middle frontal G (orbital part). L	1.62	Frontal lobe, orbital surface	Paralimbic
Inferior frontal G (triangular part). L	1.56	Frontal lobe, lateral surface	Heteromodal
Parahippocampal G .R	1.51	Limbic lobe	Paralimbic

L.: Left R.: Right G.: Gyrus.
NBC: normalized betweenness centrality.
Note: List of the hub anatomical regions (descending order of normalized betweenness centrality). These regions were classified into primary, unimodal, heteromodal, paralimbic, limbic, or subcortical as described in Mesulam (2000). See the anatomical structures localization using the AAL atlas described in Tzourio-Mazoyer et al. (2002).

There were hub regions found in the fronto-parietal regions, precuneus and superior frontal and parietal cortices, extending from the cortical midline into specific subcortical regions. Our results are in line with previous reports showing the central hub role of neocortical precuneus and superior frontal regions (Hagmann et al., 2008; Sporns et al., 2007; van den Heuvel et al., 2009) and the existence of a densely connected structural core in posterior medial cortex containing precuneus and the superior parietal cortex (Hagmann et al., 2008).

Brain regions as cingulate cortex, precuneus, cuneus, and the inferior and superior parietal cortices have also been found exhibiting elevated fiber counts and densities (node degree and strength). They are most resistant to the erosive procedures of k-core and s-core decomposition having a high topological centrality (Hagmann et al., 2008). The central structural embedding of posterior medial cortex in the human brain is consistent with a series of physiological findings including high levels of energy consumption and activation at rest (Raichle et al., 2001) and significant deactivation during goal-directed tasks (Fox et al., 2005; Raichle et al., 2001; Shulman et al., 1997). Activation of the precuneus (Cavanna and Trimble, 2006) and other cortical midline structures (Northoff and Bermpohl, 2004) has been linked to self-referential processing and consciousness. Similarly some of anatomical regions (precuneus, lateral and medial parietal cortex, and the medial prefrontal cortex) has been identified as part of human default network that comprises a set of interacting subsystems connected by hubs (Buckner et al., 2008; Fox and Raichle, 2007; Fox et al., 2005; Greicius et al., 2003).

However, in our study it was evident that hub regions (following the cortical systems classification by (Mesulam, 2000)) did not distribute topologically identical, which predominately were heteromodals (30%, precuneus and inferior frontal gyrus, pars triangularis) and paralimbics (40%, cingulate gyrus and insula). The unimodal (cuneus and superior parietal lobe) and primary (postcentral gyrus and calcarine fissure) hubs were less represented with a 20% and 10% respectively.

Our results showed left asymmetric representation of hub regions for the heteromodal cortex that play a central role receiving convergent inputs from multiple cortical regions and are most closely involved in perceptual elaboration and motor planning. On the other hand the paralimbic regions with right asymmetric topology play a critical role in channeling emotion and motivation to behaviorally relevant motor acts, mental content and extrapersonal events (Mesulam, 2000). In line with previous findings in Iturria-Medina et al. (2011a, 2011b) we suppose that hub regional asymmetries indicate that left hemisphere presents more central or indispensable regions for the whole-brain structural network than the right one. Since the connectivity of a given region is related to its cellular characteristics such as cell packing density, cell size, and number of cortical neurons (Costa and Sporns, 2005; Lerch et al., 2006), blood flow asymmetries of the cortex might be related to hemisphere specific functional specializations and metabolic demand, which is based on the high correspondence between our results and well-known structural and functional regional asymmetries seems to support the fact that the left hemisphere is 'regionally' more specialized than the right one. In terms of functional principles, these patterns appear to support the fact that the left hemisphere has a leading role for highly demanding specific process, such as language and motor actions, which may require dedicated specialized networks whereas the right hemisphere has a leading role for more general process, such as integration tasks.

Furthermore, primary regions as Calcarine fissure and surrounding cortex are represented as hub in the right hemisphere. In this respect, Cole et al. (2010) using resting state fMRI connectivity analysis show several visual regions were among the most globally connected. This may reflect the privileged placement of visual processing in the human brain (Ungerleider and Haxby, 1994).

Indeed, our analysis revealed the hub regions to be a distributed set of nodes participating in the default mode network (e.g., cingulate cortex/precuneus, medial orbitofrontal cortex), the salience network (e.g., insula, anterior cingulate cortex), the visual (cuneus) networks, and to some extent the executive control network (e.g., superior frontal and left superior parietal). One plausible explanation for the above different hub classification regions might be the tendency of the brain to provide a certain level of resilience to its core, in case of malfunction of one of its key hubs, regardless of a higher cost of the needed white matter wiring (Kaiser et al., 2007). As the hub regions are believed to handle multimodal or integrative function, their damage could dramatically affect the stability and efficiency of the network (Achard et al., 2006; Sporns and Zwi, 2004). In accordance with this view, our results confirmed that 'lesions' in the hubs lead to significantly higher changes of the path lengths as compared with 'lesions' in nonhubs.

Further considerations and future work

Some issues should be addressed in future works. The use of high resolution parcellations for an exhaustive study of the brain parcellation influences the properties of the CBF networks. Pearson correlation was adopted instead of partial correlation analysis here. The partial correlation analysis could not be performed because the sample size was not large enough for a robust estimation of this measure. The recruitment of subjects to perform SPECT experiment is difficult; therefore in the future this study should be performed for a second time to test if the CBF network properties remain using a higher number of subjects. As we recommended in previous study at this point (Sanabria-Diaz et al., 2010), it is important to answer two main questions: (1) how many subjects are needed to obtain reliable results? (2) Are comparable the results obtained by two experimenters that use samples with different number of subjects? This question would quantify subjects sample size-driven discrepancies between experimenters.

It would be very important in future work to explore how the CBF variable could detect alterations in some pathologies like Alzheimer. Also the study of anatomical/functional/CBF brain networks, by combining structural MRI, fMRI, DWI and SPECT/PET neuroimaging techniques in a same set of subjects would be tremendously useful to find differences and similar properties of brain networks obtained by different physiological cerebral variables. The used of Arterial Spin Labeling (ASL) Neuroimaging modality would be useful to study the convergence of the underlying network properties using BOLD and CBF physiological variables. Finally, it would be interesting the use of other association measures like 'Euclidean distance' to characterize different aspects of the CBF co-variations between anatomical structures and its brain topological organization.

Conclusion

This work demonstrates the presence of non-random organization of networks obtained from CBF fluctuations measured from SPECT Imaging in brain resting state. Small world architecture in this kind of networks is found, meaning there is an optimal balance between local specialization and global integration in the brain. The CBF physiological variable could be considered as a candidate variable to study the anatomical relationship between different sites as well as the network topology in brain pathologies. The possible relation between patterns of axonal (anatomical) and CBF connections is an issue that should be addressed in future works. Our results highlight the importance of examining different physiological variables to understand normal/aberrant networks properties in healthy and pathological brains.

Supplementary data to this article can be found online at http://dx.doi.org/10.1016/j.neuroimage.2012.08.082.

Acknowledgments

References

Achard, S., Bullmore, E., 2007. Efficiency and cost of economical brain functional networks. PLoS Comput. Biol. 3 (2), e17 (Feb 2).

Achard, S., Salvador, R., Whitcher, B., Suckling, J., Bullmore, E., 2006. A resilient, low-frequency, small-world human brain functional network with highly connected association cortical hubs. J. Neurosci. 26, 63–72.

Alemán-Gómez, Y., Melie-García, L., Valdes-Hernández, P., 2006. IBASPM: toolbox for automatic parcellation of brain structures. Presented at the 12th Annual Meeting of the Organization for Human Brain Mapping, June 11-15, 2006, Florence, Italy: Available on CD-Rom in NeuroImage, Vol. 27, No.1.

Bassett, D.S., Bullmore, E., 2006. Small-world brain networks. Neuroscientist 12, 512–523.

Bassett, D.S., Bullmore, E., Verchinski, B.A., Mattay, V.S., Weinberger, D.R., Meyer-Lindenberg, A., 2008. Hierarchical organization of human cortical networks in health and schizophrenia. J. Neurosci. 28, 9239–9248.

Bassettt, D.S., Meyer-Lindenberg, A., Achard, S., Duke, T., Bullmore, E., 2006. Adaptive reconfiguration of fractal small-world human brain functional networks. Proc. Natl. Acad. Sci. U. S. A. 103, 19518–19523.

Biswal, B.B., VanKylen, J., Hyde, J.S., 1997. Simultaneous assessment of flow and BOLD signals in resting-state functional connectivity maps. NMR Biomed. 10, 165–170.

Boccaletti, S., Latora, V., Moreno, Y., Chavez, M., Hwang, D.-U., 2006. Complex networks: structure and dynamics, pp. 175–308.

Buckner, R.L., Andrews-Hanna, J.R., Schacter, D.L., 2008. The brain's default network: anatomy, function, and relevance to disease. Ann. N. Y. Acad. Sci. 1124, 1–38.

Bullmore, E., Sporns, O., 2009. Complex brain networks: graph theoretical analysis of structural and functional systems. Nat. Rev. Neurosci. 10, 186–198.

Buxton, R.B., Uludag, K., Dubowitz, D.J., Liu, T.T., 2004. Modeling the hemodynamic response to brain activation. Neuroimage 23, S220–S233.

Cavanna, A.E., Trimble, M.R., 2006. The precuneus: a review of its functional anatomy and behavioural correlates. Brain 129, 564–583.

Chang, L.T., 1978. A method for attenuation correction in radionuclide computed tomography. IEEE Trans Nucl Sci NS 25, 638–644.

Chen, Z.J., He, Y., Rosa-Neto, P., Germann, J., Evans, A.C., 2008. Revealing modular architecture of human brain structural networks by using cortical thickness from MRI. Cereb. Cortex 18, 2374–2381.

Chuang, K.H., Van Gelderen, P., Merkle, H., Bodurka, J., Ikonomidou, V.N., Koretsky, A.P., Duyn, J.H., Talagala, S.L., 2008. Mapping resting-state functional connectivity using perfusion MRI. Neuroimage 40, 1595–1605.

Cole, M.W., Pathak, S., Schneider, W., 2010. Identifying the brain's most globally connected regions. Neuroimage 49, 3132–3148.

Costa, L.daF., Sporns, O., 2005. Hierarchical features of large-scale cortical connectivity, 48 ed. , pp. 567–573.

De Luca, M., Beckmann, C.F., De Stefano, N., Matthews, P.M., Smith, S.M., 2006. fMRI resting state networks define distinct modes of long-distance interactions in the human brain. Neuroimage 29, 1359–1367.

DeKosky, S.T., Scheff, S.W., 1990. Synapse loss in frontal cortex biopsies in Alzheimer's disease: correlation with cognitive severity. Ann. Neurol. 27, 457–464.

Detre, J.A., Leigh, J.S., Williams, D.S., Koretsky, A.P., 1992. Perfusion imaging. Magn. Reson. Med. 23, 37–45.

Deuker, L., Bullmore, E.T., Smith, M., Christensen, S., Nathan, P.J., Rockstroh, B., Bassett, D.S., 2009. Reproducibility of graph metrics of human brain functional networks. Neuroimage 47, 1460–1468.

Eguiluz, V.M., Chialvo, D.R., Cecchi, G.A., Baliki, M., Apkarian, A.V., 2005. Scale-free brain functional networks. Phys. Rev. Lett. 94, 018102.

Fox, M.D., Raichle, M.E., 2007. Spontaneous fluctuations in brain activity observed with functional magnetic imaging. Nat. Rev. Neurosci. 700–711.

Fox, M.D., Snyder, A.Z., Vincent, J.L., Corbetta, M., Van, E., Raichle, M.E., 2005. The human brain is intrinsically organized into dynamic, anticorrelated functional networks. Proc. Natl. Acad. Sci. U. S. A. 102, 9673–9678.

Friston, K.J., Frith, C.D., Liddle, P.F., Frackowiak, R.S.J., 1993. Functional connectivity — the principal-component analysis of large (Pet) data sets. J. Cereb. Blood Flow Metab. 13, 5–14.

Gómez-Padrón, I., Silva Loynaz, C., Seuc Chiu, A., 1985. Anatomía II. Folleto complementario. Ministerio de salud pública, Cuba.

Gong, G., Rosa-Neto, P., Carbonell, F., Chen, Z.J., He, Y., Evans, A.C., 2009. Age- and gender-related differences in the cortical anatomical network. J. Neurosci. 29, 15684–15693.

Greicius, M.D., Krasnow, B., Reiss, A.L., Menon, V., 2003. Functional connectivity in the resting brain: a network analysis of the default mode hypothesis. Proc. Natl. Acad. Sci. U. S. A. 100, 253–258.

Hagmann, P., Kurant, M., Gigandet, X., Thiran, P., Wedeen, V.J., Meuli, R., Thiran, J.P., 2007. Mapping human whole-brain structural networks with diffusion MRI. PLoS One 2.

Hagmann, P., Cammoun, L., Gigandet, X., Meuli, R., Honey, C.J., Wedeen, V., Sporns, O., 2008. Mapping the structural core of human cerebral cortex. PLoS Biol. 6, 1479–1493.

Hampson, M., Peterson, B.S., Skudlarski, P., Gatenby, J.C., Gore, J.C., 2002. Detection of functional connectivity using temporal correlations in MR images. Hum. Brain Mapp. 15, 247–262.

He, Y., Chen, Z.J., Evans, A.C., 2007a. Small-world anatomical networks in the human brain revealed by cortical thickness from MRI. Cereb. Cortex 17, 2407–2419.

He, Y., Wang, L., Zang, Y.F., Tian, L.X., Zhang, X.Q., Li, K.C., Jiang, T.Z., 2007b. Regional coherence changes in the early stages of Alzheimer's disease: A combined structural and resting-state functional MRI study. Neuroimage 35, 488–500.

He, Y., Chen, Z., Evans, A., 2008. Structural insights into aberrant topological patterns of large-scale cortical networks in Alzheimer's disease. J. Neurosci. 28, 4756–4766.

He, Y., Chen, Z., Gong, G., Evans, A., 2009a. Neuronal networks in Alzheimer's disease. Neuroscientist 15, 333–350.

He, Y., Dagher, A., Chen, Z., Charil, A., Zijdenbos, A., Worsley, K., Evans, A., 2009b. Impaired small-world efficiency in structural cortical networks in multiple sclerosis associated with white matter lesion load. Brain 132, 3366–3379.

Hilgetag, C.C., Kaiser, M., 2004. Clustered Organization of Cortical Connectivity, 2 ed. , pp. 353–360.

Hofer, S., Frahm, J., 2006. Topography of the human corpus callosum revisited—comprehensive fiber tractography using diffusion tensor magnetic resonance imaging. Neuroimage 32, 989–994.

Holman, B.L., Tumeh, S.S., 1990. Single-photon emission computed tomography (SPECT). Applications and potential. JAMA 263, 561–564.

Huang, H., Zhang, J., Jiang, H., Wakana, S., Poetscher, L., Miller, M.I., van Zijl, P.C., Hillis, A.E., Wytik, R., Mori, S., 2005. DTI tractography based parcellation of white matter: application to the mid-sagittal morphology of corpus callosum. Neuroimage 26, 195–205.

Iturria-Medina, Y., Sotero, R.C., Canales-Rodriguez, E.J., Aleman-Gomez, Y., Melie-Garcia, L., 2008. Studying the human brain anatomical network via diffusion-weighted MRI and Graph Theory. Neuroimage 40, 1064–1076.

Iturria-Medina, Y., Perez, F.A., Morris, D.M., Canales-Rodriguez, E.J., Haroon, H.A., Garcia, P.L., Augath, M., Galan, G.L., Logothetis, N., Parker, G.J., Melie-Garcia, L., 2011a. Brain hemispheric structural efficiency and interconnectivity rightward asymmetry in human and nonhuman primates. Cereb. Cortex 21, 56–67.

Iturria-Medina, Y., Perez Fernandez, A., Valdes Hernandez, P., Garcia Penton, L., Canales-Rodriguez, E.J., Melie-Garcia, L., Lage Castellanos, A., Ontivero Ortega, M., 2011b. Automated discrimination of brain pathological state attending to complex structural brain network properties: the shiverer mutant mouse case. PLoS One 6.

Jellison, B.J., Field, A.S., Medow, J., Lazar, M., Salamat, M.S., Alexander, A.L., 2004. Diffusion tensor imaging of cerebral white matter: a pictorial review of physics, fiber tract anatomy, and tumor imaging patterns. Am. J. Neuroradiol. 25, 356–369.

Kaiser, M., Martin, R., Andras, P., Young, M.P., 2007. Simulation of robustness against lesions of cortical networks. Eur. J. Neurosci. 25, 3185–3192.

Lassen, N.A., Andersen, A.R., Friberg, L., Paulson, O.B., 1988. The retention of [99mTc]-d, l-HM-PAO in the human brain after intracarotid bolus injection: a kinetic analysis. J. Cereb. Blood Flow Metab. 8, S13–S22.

Lerch, J.P., Worsley, K., Shaw, W.P., Greenstein, D.K., Lenroot, R.K., Gledd, J., Evans, A.C., 2006. Mapping anatomical correlations across cerebral cortex (MACACC) using cortical thickness from MRI. Neuroimage 31, 993–1003.

Liu, Y., Liang, M., Zhou, Y., He, Y., Hao, Y.H., Song, M., Yu, C.S., Liu, H.H., Liu, Z.N., Jiang, T.Z., 2008. Disrupted small-world networks in schizophrenia. Brain 131, 945–961.

Lowe, M.J., Mock, B.J., Sorenson, J.A., 1998. Functional connectivity in single and multislice echoplanar imaging using resting-state fluctuations. Neuroimage 7, 119–132.

Makris, N., Kennedy, D.N., McInerney, S., Sorensen, A.G., Wang, R., Caviness Jr., V.S., Pandya, D.N., 2005. Segmentation of subcomponents within the superior longitudinal fascicle in humans: a quantitative, in vivo, DT-MRI study. Cereb. Cortex 15, 854–869.

Mechelli, A., Friston, K.J., Frackowiak, R.S., Price, C.J., 2005. Structural covariance in the human cortex. J. Neurosci. 25, 8303–8310.

Mesulam, M.M., 2000. Principles of Behavioral and Cognitive Neurology. OXFOR University Press, Oxfor.

Micheloyannis, S., Pachou, E., Stam, C.J., Breakspear, M., Bitsios, P., Vourkas, M., Erimaki, S., Zervakis, M., 2006. Small-world networks and disturbed functional connectivity in schizophrenia. Schizophr. Res. 87, 60–66.

Northoff, G., Bermpohl, F., 2004. Cortical midline structures and the self. Trends Cogn. Sci. 8, 102–107.

Okabe, S., Hanajima, R., Ohnishi, T., Nishikawa, M., Imabayashi, E., Takano, H., Kawachi, T., Matsuda, H., Shiio, Y., Iwata, N.K., Furubayashi, T., Terao, Y., Ugawa, Y., 2003. Functional connectivity revealed by single-photon emission computed tomography (SPECT) during repetitive transcranial magnetic stimulation (rTMS) of the motor cortex. Clin. Neurophysiol. 114, 450–457.

Petrides, M., 2005. Lateral prefrontal cortex: architectonic and functional organization. Philos. Trans. R. Soc. Lond. B Biol. Sci. 360, 781–795.

Quarantelli, M., Berkouk, K., Prinster, A., Landeau, B., Svarer, C., Balkay, L., Alfano, B., Brunetti, A., Baron, J.C., Salvatore, M., 2004. Integrated software for the analysis of brain PET/SPECT studies with partial-volume-effect correction. J. Nucl. Med. 45, 192–201.

Raichle, M.E., 2006. Neuroscience. The brain's dark energy. Science 314, 1249–1250.

Raichle, M.E., MacLeod, A.M., Snyder, A.Z., Powers, W.J., Gusnard, D.A., Shulman, G.L., 2001. A default mode of brain function. Proc. Natl. Acad. Sci. U. S. A. 98, 676–682.

Rubinov, M., Sporns, O., 2010. Complex network measures of brain connectivity: uses and interpretations. Neuroimage 52, 1059–1069.

Salvador, R., Suckling, J., Coleman, M.R., Pickard, J.D., Menon, D., Bullmore, E., 2005. Neurophysiological architecture of functional magnetic resonance images of human brain. Cereb. Cortex 15, 1332–1342.

Sanabria-Diaz, G., Melie-Garcia, L., Iturria-Medina, Y., Eman-Gomez, Y., Hernandez-Gonzalez, G., Valdes-Urrutia, L., Galan, L., Valdes-Sosa, P., 2010. Surface area and cortical thickness descriptors reveal different attributes of the structural human brain networks. Neuroimage 50, 1497–1510.

Shulman, G.L., Fiez, J.A., Corbetta, M., Buckner, R.L., Miezin, F.M., Raichle, M.E., Petersen, S.E., 1997. Common blood flow changes across visual tasks.2. Decreases in cerebral cortex. J. Cogn. Neurosci. 9, 648–663.

Sporns, O., Kotter, R., 2004. Motifs in brain networks. PLoS Biol. 2.

Sporns, O., Zwi, J.D., 2004. The small world of the cerebral cortex. Neuroinformatics 2, 145–162.

Sporns, O., Tononi, G., Edelman, G.M., 2000. Connectivity and complexity: the relationship between neuroanatomy and brain dynamics. Neural Netw. 13, 909–922.

Sporns, O., Honey, C.J., Kotter, R., 2007. Identification and classification of hubs in brain networks. PLoS One 2.

Stam, C.J., 2004. Functional connectivity patterns of human magnetoencephalographic recordings: a 'small-world' network? Neurosci. Lett. 355, 25–28.

Stam, C.J., Reijneveld, J.C., 2007. Graph theoretical analysis of complex networks in the brain. Nonlinear. Biomed. Phys. 1, 3.

Stam, C.J., Jones, B.F., Nolte, G., Breakspear, M., Scheltens, P., 2007. Small-world networks and functional connectivity in Alzheimer's disease. Cereb. Cortex 17, 92–99.

Standring, S., 2004. Gray's Anatomy: The Anatomical Basis of Medicine and Surgery, 39th edition. Churchill Livingstone.

Stark, D.E., Margulies, D.S., Shehzad, Z.E., Reiss, P., Kelly, A.M., Uddin, L.Q., Gee, D.G., Roy, A.K., Banich, M.T., Castellanos, F.X., Milham, M.P., 2008. Regional variation in interhemispheric coordination of intrinsic hemodynamic fluctuations. J. Neurosci. 28, 13754–13764.

Toga, A.W., Thompson, P.M., 2003. Mapping brain asymmetry. Nat. Rev. Neurosci. 4, 37–48.

Tzourio-Mazoyer, N., Papathanassiou, D., Crivello, F., Etard, O., Delcroix, N., Mayozer, B., Joliot, M., 2002. Automated Anatomical Labeling of Activations in SPM Using a Macroscopic Anatomical Parcellation of the MNI MRI Single-Subject Brain, 15 ed. , pp. 273–289.

Ungerleider, L.G., Haxby, J.V., 1994. 'What' and 'where' in the human brain. Curr. Opin. Neurobiol. 4, 157–165.

van den Heuvel, M.P., Sporns, O., 2011. Rich-club organization of the human connectome. J. Neurosci. 31, 15775–15786.

van den Heuvel, M.P., Stam, C.J., Boersma, M., Hulshoff Pol, H.E., 2008. Small-world and scale-free organization of voxel-based resting-state functional connectivity in the human brain. Neuroimage 43, 528–539.

van den Heuvel, M.P., Mandl, R.C., Kahn, R.S., Hulshoff Pol, H.E., 2009. Functionally linked resting-state networks reflect the underlying structural connectivity architecture of the human brain. Hum. Brain Mapp. 30, 3127–3141.

Varkuti, B., Cavusoglu, M., Kullik, A., Schiffler, B., Veit, R., Yilmaz, O., Rosenstiel, W., Braun, C., Uludag, K., Birbaumer, N., Sitaram, R., 2011. Quantifying the link between anatomical connectivity, gray matter volume and regional cerebral blood flow: an integrative MRI study. PLoS One 6.

Viviani, R., Messina, I., Walter, M., 2011. Resting state functional connectivity in perfusion imaging: correlation maps with BOLD connectivity and resting state perfusion. PLoS One 6.

Wakana, S., Jiang, H., Nagae-Poetscher, L.M., van Zijl, P.C., Mori, S., 2004. Fiber tract-based atlas of human white matter anatomy. Radiology 230, 77–87.

Wang, L., Zang, Y.F., He, Y., Liang, M., Zhang, X.Q., Tian, L.X., Wu, T., Jiang, T.Z., Li, K.C., 2006. Changes in hippocampal connectivity in the early stages of Alzheimer's disease: evidence from resting state fMRI. Neuroimage 31, 496–504.

Wang, J.H., Wang, L., Zang, Y.F., Yang, H., Tang, H.H., Gong, Q.Y., Chen, Z., Zhu, C.Z., He, Y., 2009. Parcellation-dependent small-world brain functional networks: a resting-state fMRI study. Hum. Brain Mapp. 30, 1511–1523.

Wintermark, M., Sesay, M., Barbier, E., Borbely, K., Dillon, W.P., Eastwood, J.D., Glenn, T.C., Grandin, C.B., Pedraza, S., Soustiel, J.F., Nariai, T., Zaharchuk, G., Caille, J.M., Dousset, V., Yonas, H., 2005. Comparative overview of brain perfusion imaging techniques. J. Neuroradiol. 32, 294–314.

Witelson, S.F., 1989. Hand and sex differences in the isthmus and genu of the human corpus callosum. A postmortem morphological study. Brain 112 (Pt 3), 799–835.

Wu, C.W., Gu, H., Lu, H., Stein, E.A., Chen, J.H., Yang, Y., 2009. Mapping functional connectivity based on synchronized CMRO(2) fluctuations during the resting state. Neuroimage 45, 694–701.

Yao, Z., Zhang, Y., Lin, L., Zhou, Y., Xu, C., Jiang, T., 2010. Abnormal cortical networks in mild cognitive impairment and Alzheimer's disease. PLoS Comput. Biol. 6, e1001006.

Zarei, M., Johansen-Berg, H., Smith, S., Ciccarelli, O., Thompson, A.J., Matthews, P.M., 2006. Functional anatomy of interhemispheric cortical connections in the human brain. J. Anat. 209, 311–320.

Zou, Q., Wu, C.W., Stein, E.A., Zang, Y., Yang, Y., 2009. Static and dynamic characteristics of cerebral blood flow during the resting state. Neuroimage 48, 515–524.